TRF2 promotes dynamic and stepwise looping of POT1 bound telomeric overhang

Tapas Paul
Johns Hopkins University
Wilson Liou
Johns Hopkins University
Xinyi Cai
Johns Hopkins University
Patricia Opresko
North Carolina State University
Sua Myong (smyong@jhu.edu)
Johns Hopkins University https://orcid.org/0000-0001-9098-3423

Article

Keywords: Conformational Dynamics, Loop Formation, Duplex-single Stranded Junction

Posted Date: September 22nd, 2020

DOI: https://doi.org/10.21203/rs.3.rs-79038/v1

Version of Record: A version of this preprint was published at Nucleic Acids Research on January 1st, 2021. See the published version at https://doi.org/10.1093/nar/gkab1123.

Abstract

Human telomeres are protected by shelterin components including POT1 and TRF2 but the molecular mechanism remains elusive. Here, we report an unexpected activity of POT1 in imparting conformational dynamics of the telomere overhang, even at a monomer level. Such POT1 induced overhang dynamics is greatly enhanced when TRF2 engages with the telomere duplex. Strikingly, TRF2 brings a POT1 bound overhang to the duplex and induces a stepwise movement up and down the axis of telomere duplex, thereby generating a highly dynamic loop formation. Interestingly, TRF2, but not TRF2ΔB, recruits POT1 bound overhang to the telomere duplex-single stranded junction by discrete steps of movement with a step size of TTAGGG. The same steps are observed regardless of the length of the POT1 bound overhang, suggesting a tightly regulated mechanism. Based on our results, we propose a plausible dynamic mechanism of t-loop formation coordinated by POT1 and TRF2.

Introduction

Eukaryotic chromosomal ends are capped by DNA-protein complexes termed telomeres, which can prevent chromosomal degradation, end-to-end fusions and is essential for genome stability[1-3]. Human telomeric DNA is composed of 2 to 20 kb of duplexed tandem TTAGGG repeats followed by 75-300 nucleotides of the same TTAGGG repeats at 3' overhang which can fold into G-quadruplex (G4)[4-7]. The shelterin complex contain six subunits of proteins including TRF1, TRF2, RAP1, TIN2, TPP1, and POT1 that protect the chromosomal ends by physically associating with each other and the telomeric repeats[1,8-10]. Among the six shelterin subunits, TRF1, TRF2 and POT1 specifically recognize and directly bind double- and single-stranded TTAGGG repeats, respectively. They bind telomeric DNA independently without rendering cooperativity to each other[1,9]. TIN2 interacts with both TRF1 and TRF2, whereas TPP1 forms a heterodimer with POT1 and links with TIN2[10-12]. Shelterin complex is located along the telomere and displays a strong affinity for binding at double-/single-stranded telomeric junction[1,9,10]. Evidences indicate that shelterin may not be a static structure[1,9,13], consistent with the known functions of shelterin. Telomeres and shelterin proteins allow cells to distinguish natural chromosome ends from the damaged DNA[2,3,14]. Upon loss or disruption of shelterin, telomeres associate with at least seven distinct DNA damage response pathways including p53 dependent apoptosis[9,15-17]. Hence, telomere maintenance by shelterin proteins is essential for normal cell growth and its dysregulation may have direct consequences in aging and cancer[18].

The telomeric single-stranded overhang is critical for proper telomere function[7,19,20]. POT1 is the only shelterin component that specifically binds telomeric overhangs with nanomolar affinity and is essential for telomere integrity[21,22]. A high-resolution crystal structure revealed that human POT1 contains two oligonucleotide-binding folds (OB1 and OB2), tightly engaged with 10 nucleotides, 'TTAGGGTTAG' with an exceptionally high sequence specificity[23]. OB1 makes extensive contact with the first six nucleotides whereas OB2 binds the other four nucleotides, producing a sharp 90° kink in the DNA backbone. Two POT1 molecules are expected to bind and unfold one intramolecular telomeric G4 structure[24-26]. Further,

multiple POT1 units associate with longer telomeric ssDNA, leaving a ‘GG’ gap in between two successive units[23,27]. While structural and biochemical studies reveal the exquisite POT1-DNA contact in atomic resolution and well-defined stoichiometry of the complex, it remains unknown if the POT1 bound telomere overhangs is static or dynamic in nature and if it makes contact with the telomeric duplex coated with other shelterin components.

TRF2 exclusively binds telomeric duplex ‘TAGGGTT’ with a nanomolar affinity[9-11]. The abundance of the core shelterin is sufficient to bind all duplex TTAGGG repeats although in vivo concentrations of each components are variable[9,14,28]. Further evidence suggests that TRF2, but not TRF1 plays a significant role in protecting and maintaining the integrity of the telomere structure[29]. The end of the telomere is wrapped up in a special structure termed t-loop which is a large lariat structure generated by the invasion of the 3’ G-rich overhang into the telomeric dsDNA. The G-rich overhang pairs up with C-rich strand in the duplex and displaces the G-rich strand to form a D-loop structure[30-32]. The formation of t-loop requires both a TTAGGG overhang and duplex as blunt-ended telomeres cannot form t-loops[31]. TRF2 is capable of converting the un-looped telomeric DNA into t-loop along the telomeric dsDNA[1,9,32]. Telomere looping is a common theme in telomere architecture and is observed in all stages of the cell cycle[9,31] and telomere looping dynamics protect the chromosome end[33]. The question still remains regarding how TRF2 contributes to the t-loop formation. It has been proposed that TRF2 may search for partner proteins through diffusion and stabilize the interaction with specific telomeric DNA[13,34].

Two shelterin components, POT1 and TRF2, confer the highest sequence specificity to telomeric overhang and duplex binding, respectively. Both are also critical for the t-loop formation and overall telomere function. TRF2 preferentially binds the telomeric single strand and duplex junction and is capable of remodelling telomeric DNA into t-loops[31,32]. POT1 engages with telomeric overhang as well as the t-loop[9,31,32]. TRF2 and POT1 cooperate to maintain telomere integrity[35], regulate telomere length[36], participate in telomere capping[35] and protect telomeres from ATM and ATR DNA damage response[14]. TRF2 may play a dominant role in t-loop formation[37], yet the mechanistic role played by TRF2 and POT1 remain unclear. Here we report that unexpectedly, the POT1-overhang complex is inherently dynamic, making frequent contact with the duplex DNA *in cis*. Remarkably, such POT1-overhang dynamics is dramatically increased when TRF2 is engaged with the telomeric duplex. The motion entails dynamic looping-unlooping transitions which exhibits distinct stepwise movement coordinated by both proteins. We deduced the step size or contact site of one TTAGGG repeat along the axis of telomeric duplex. The looped state is more stabilized with increasing length of POT1 bound overhang. We propose a plausible mechanism by which POT1 and TRF2 may coordinate to form the t-loop.

Results

POT1 remains stably bound to telomere overhangs

POT1 is a unique protein in that it binds exclusively to telomere overhangs with high affinity and sequence specificity in a well-defined structural organization[23]. Previously, we showed that POT1 domains associate with human telomeric overhang $(TTAGGG)_4$ sequentially, one oligonucleotide/oligosaccharide binding (OB) fold at a time[24]. Here, we asked if the POT1 bound telomere overhang remains stably engaged without dissociation or conformational dynamics over time. For this goal, we varied the FRET dye positions to assess the status of the POT1-overhang complex more accurately. As we published previously, the substrate contained telomeric ssDNA composed of four TTAGGG repeats, or 4R (forms one complete G4) and an 18 bp duplex for immobilization via biotin-NeutrAvidin to a slide[24]. We use "G4" and "4R" to denote G-quadruplex and four repeats of TTAGGG, respectively. The construct consisted of a donor (Cy3) dye at the 3' end and the acceptor (Cy5) dye labelled in-between the 4^{th} and 5^{th} base pair from the double-/single-strand (ds/ss) junction, hence termed Top4.5 (Fig. 1a). FRET histograms were built by collecting FRET values from more than 4000 molecules in 20 different fields of view. The 4R exhibits a mid-FRET peak ~0.65 due to the folded G4 and the 4.5 bp spacing from the ds/ss junction (Fig. 1b). After the addition of POT1 (25 nM), the mid-FRET peak completely shifted to low FRET at ~0.3, indicating complete binding of POT1 (Fig. 1b). To test how stable the POT1-overhang complex is, we performed a competition assay by applying a molar excess (>10x) of unlabelled 4R (no 18 bp), C4 (complementary sequence of $[TTAGGG]_4$), and 100 mM KCl (G4 stabilizing condition, POT1 doesn't bind overhangs at 100 mM KCl)[26,38] to the POT1 bound overhang. After 30 minutes of incubation, the FRET histogram remained unchanged at FRET~0.3 in every case (Fig. 1c), clearly indicating the exceptional stability of POT1-overhang complex.

Real-time POT1 binding to 4R/G4 revealed a clear mid FRET to low FRET transition immediately after the POT1 addition (Fig. 1d). More than 100 single-molecule traces were combined to generate a heatmap in which each trace was synchronized at the moment of FRET decrease (Fig. 1e). The quick transition from free G4 (~0.65 FRET) to the POT1 bound state (~0.3 FRET) indicates a rapid POT1 binding to the telomere overhang. Furthermore, we obtained smFRET traces that exhibit one (~52%), two (~33%), three (~<10%), and four (~<10%) steps of POT1 binding (Supplementary Fig. 1). The stepwise FRET decrease corresponds to the OB folds of POT1 binding sequentially, which is consistent with our previous finding[24]. For kinetic analysis, varying concentrations of POT1 from 0.1 nM to 50 nM was applied to FRET labelled G4. The binding time was calculated based on the dwell time between POT1 addition and the subsequent FRET decline from the smFRET traces (for [POT1] > 10 nM). For low concentrations, due to slower binding, we used the bound fraction calculated from FRET histograms taken over time (for [POT1] < 10 nM). The binding rates were determined by exponentially fitting the bound fractions with respect to time (Fig. 1f). The rate exponentially decreased as the protein concentration decreased (Fig. 1g). The equilibrium dissociation constant (K_D) was determined to be 1.51 ± 0.26 nM (Fig. 1h), confirming an extremely high affinity of POT1 to telomere overhang.

POT1 bound telomeric overhang displays dynamic motion

The above observation demonstrates that two POT1 monomers are stably engaged with the telomeric G4 overhang. To check if such a stable interaction is maintained over time, we looked through single-molecule traces taken before and after washing off unbound POT1. In both conditions, while some traces showed a steady FRET at ~0.3 which corresponds to the steady POT1 bound state (Fig. 2a), surprisingly, many traces displayed FRET fluctuations, indicating a dynamic state of the POT1-overhang complex. Among the dynamic traces, we found two different patterns categorized as Dynamic-I and –II based on the FRET fluctuation pattern. Dynamic-I includes traces that show slower FRET fluctuations oscillating between ~0.2 and 0.6 whereas Dynamic-II contains sharp FRET peaks that reaches above ~0.6 FRET, often rising up to 0.9 which is higher than the G4-only FRET (Fig. 2a, more traces, in Supplementary Fig. 2a). Dynamic-I+II refer to traces that had mixture of the both dynamic patterns. These dynamics spikes occur stochastically, varying in frequency. The dynamics are observed immediately after POT1 binding as shown in the real-time smFRET traces (Supplementary Fig. 2b). Based on the criteria stated above, we categorized over 1000 smFRET traces into steady, Dynamic-I and –II. Approximately, ~40-45% were steady while ~30-35% was Dynamic-I and ~25-30%, Dynamic-II (Fig. 2b). To check if the dynamics are concentration dependent, we titrated the protein to concentrations ranging from 1 nM to 50 nM. Remarkably, the distribution of steady vs. dynamic pattern remained the same in all POT1 concentrations both before and after the wash of free protein (Fig. 2c). Taken together with the stable association of POT1 to the telomere overhang (Fig. 1c), this clearly indicates that the POT1 induced conformational dynamics arise from the stably bound configuration rather than binding and unbinding events. Next, we analyzed the dwell time representing the frequency of FRET fluctuation and found that Dynamic-I ($\delta t1$ = 2.51 ± 0.31 sec) is ~ four-fold slower than the Dynamic-II ($\delta t2$ = 0.63 ± 0.14 sec), consistent with the long- and short-lived excursions seen in Dynamic-I and –II, respectively (Fig. 2d).

To further probe the POT1 induced conformational dynamics at the telomeric overhang, we modified the FRET DNA construct by repositioning the acceptor dye to the top of the duplex (Top0) in one construct and in-between the 7^{th} and 8^{th} base pairs (Top7.5) in another (Fig. 2e & f). POT1 was applied to both constructs and the smFRET traces were examined after washing out free protein. Both constructs showed dynamic FRET albeit with less pronounced FRET change than the case of Top4.5 construct (Fig. 2e & f). While the smFRET traces for Top0 (FRET ~0.4, POT1 bound state) showed FRET decreases to 0.2 and increases to ~0.7, the Top7.5 traces (FRET ~0.2, POT1 bound state) displayed only FRET increases to ~0.5. To compare the overall FRET fluctuation range exhibited in the three DNA constructs, we generated a heatmap depicting the FRET fluctuation dynamics collected from over 200 smFRET traces in each condition (Fig. 2g). The major FRET level (brightest band) is different for the three constructs due to the different dye positions despite the same POT1 induced state. Interestingly, the Top4.5 displays the widest span of FRET values (0.15-0.9) compared to the other two. Top0 and Top7.5 each shows FRET range between 0.2-0.7 and 0.1-0.6, respectively. Such difference in FRET range serves as a proxy for the path taken by the mobile POT1-overhang complex with respect to the duplex DNA.

Taken together, the POT1 bound telomeric 4R overhang is not a static structure, but a highly dynamic complex. The unexpected high FRET of 0.9 shown at the Top4.5 construct indicates that the 3’ end of

POT1-overhang approaches the 4-5th base pair of duplex to an extremely close proximity, approximately within 3 nanometers. This result suggests a transient and dynamic loop formed by POT1 bound telomere overhang as depicted in Fig. 2h.

The monomer POT1 bound telomeric overhang displays a dynamic state

Next, we asked if the dynamic conformational change arises from the dimer bound state since the structure predicts two guanine spacing between the two tandem binding of POT1 molecules [23], which can serve as a pivot point for the observed motion. To test this, we examined a monomer POT1 bound condition on a shortened overhang construct composed of two repeats of TTAGGG (2R) with the same Top4.5 acceptor dye arrangement which should only allow for one POT1 binding (Fig. 3a). Due to the short length of overhang, the DNA yields ~0.9 FRET which immediately shifted to ~0.6 FRET upon POT1 addition (Fig. 3b). The K_D of POT1 for 2R was 1.35 ± 0.32 nM, which is 5-fold tighter than previously reported[23] and comparable to the affinity toward 4R overhang (Fig. 3c). The smFRET traces showed mixture of a constant 0.6 FRET corresponding to the steady binding state, and oscillating FRET between 0.6 and 0.3 as the dynamic state (Fig. 3d, more traces in Supplementary Fig. 3). Considering the 0.6 FRET as the POT1 monomer bound state and 0.3 as lower than the 0.5 FRET observed in unfolded poly dT12 substrates (same length as 2R)[39], fluctuation between 0.6 and 0.3 indicate that the 3' telomeric end displays excursions to a fully extended conformation (depicted in Fig. 3g). As done for 4R, we quantified the fraction of steady vs. dynamic traces and found ~40% steady and ~60% dynamic behavior, which is similar to the case of two POT1 monomers bound to the 4R overhang (Fig. 3e). The dwell time collected from the dynamic FRET transitions (δt1 = 2.31 ± 0.29 sec) was similar to the Dynamic-I obtained for 4R overhang (δt1 = 2.51 ± 0.31 sec) (Fig. 3f), likely suggesting that Dynamic-I represented a monomer mediated conformational change while Dynamic-II arose from the two monomers bound state. Altogether, the POT1-overhang induced dynamics occurs even at the monomer level, likely entailing full straightening of the 2R overhang which may be accompanied by stretching out or unbending of OB1 and OB2 domains within a monomer (Fig. 3g).

TRF2 enhances POT1 induced overhang dynamics

Results so far suggest that the POT1 bound telomeric overhang undergoes dynamic conformational change at both monomer and dimer levels. Next, we asked if such behaviour changes upon TRF2 binding to telomeric duplex *in cis* as both POT1 and TRF2 are involved in the telomere end protection by forming a lariat D-/T-loop structure[32]. To test this hypothesis, we extended the dsDNA by inserting four TTAGGG repeats of telomeric duplex to the Top4.5 construct (Fig. 4a). First, we checked if telomeric duplex has any impact on POT1 induced dynamics. We performed the identical POT1 binding assay and found that the FRET pattern is highly similar to the non-telomeric duplex with 4R (Fig. 4b), including nearly indistinguishable distribution and kinetics of Dynamic-I and –II (Supplementary Fig. 4). Hence, we confirm that telomeric duplex doesn't modulate POT1 induced telomere overhang dynamics.

The shelterin component, TRF2 binds telomeric duplex as a homodimer with a high sequence specificity of “TAGGGTT”[9,10]. Thus, one TRF2 homodimer occupies two TTAGGG telomeric duplex repeats, matching the length requirement of one POT1 binding on the overhang. When TRF2 (25 nM) was added to the DNA with telomeric duplex (Fig. 4a), the FRET peak at 0.65 remained the same, making it impossible to check for binding (Fig. 4b). The lack of FRET change may be due to either no binding or binding without altering the FRET value. To test this more directly, we used an alternative approach, protein-induced fluorescence enhancement (PIFE)[40,41]. We tested TRF2 binding by performing PIFE experiments of both Cy5 and Cy3 excitation and observed a clear PIFE effect immediately after TRF2 addition, indicating a rapid binding of TRF2 (binding rate ~ 0.13 ± 0.2 sec^{-1}) (Supplementary Fig. 5). Therefore, TRF2 binds telomeric duplex without changing the G4 conformation, consistent with previous findings[10,11].

Next, we tested the POT1-overhang dynamics in the presence of TRF2 bound to the telomeric duplex. POT1 and TRF2 were added sequentially to our smFRET construct. When TRF2 was added to the POT1 bound state, the FRET peak at ~0.3 (POT1 bound state) appeared with a slightly broader width, likely indicating the TRF2 impact on the POT1 bound overhang (Fig. 4b). Strikingly, the smFRET traces revealed remarkably higher occurrence of both Dynamic –I and -II states than the case without TRF2 (Fig. 4c, d). The trace classification yielded ~20% steady, ~45% Dynamic-I, and ~ 35% Dynamic-II, altogether comprising ~80% dynamic motion, compared to 60% in POT1 alone without TRF2 (Fig. 4d). The enhanced frequency of dynamics strongly indicates the influence of TRF2 in reinforcing the POT1 induced overhang dynamics with the duplex. To check how long it takes for TRF2 to impart its modulation of POT1 bounds overhang dynamics, we examined real-time smFRET traces which were collected from the time before the TRF2 addition to approximately 3 minutes afterwards. Overall, we observed a rapid FRET increase immediately after the TRF2 addition, followed by robust FRET fluctuations seen in a majority of the traces (Fig. 4e). To demonstrate this effect collectively, we generated a heatmap by combining real-time dynamic traces (>50) (Fig. 4f, bottom). Such effect was not observed in the absence of TRF2 (Fig. 4f, top) or on non-telomeric duplex (Supplementary Fig. 6). This suggests TRF2 does not interact with non-telomeric duplex or directly with POT1 in the absence of telomeric duplex. Therefore, TRF2 promotes POT1 induced overhang dynamics only in the context of the TRF2 bound telomeric duplex.

TRF2-POT1 induced dynamics is independent of overhang length

Based on the results above, we hypothesized that the frequent contact made between the POT1 bound overhang and duplex associated TRF2 may represent a transient, yet persistent loop forming activity. We reasoned that if such looping motion is coordinated by POT1 and TRF2, similar movement may persist even when the overhang length is extended. On the contrary, if the motion was rather a random fluctuation, the longer overhang of 6 to 8 repeats will less likely be in the FRET sensitive distance range. To test this, we lengthened the telomeric overhang from four TTAGGG repeats (4R) to six (6R) and eight repeats (8R) while keeping the same four repeats of telomeric duplex. POT1 binding to 6R and 8R

overhangs yielded low FRET ~0.2, consistent with the POT1 bound state [42]. The smFRET traces obtained in POT1 bound state showed dynamics, but with diminished FRET range, likely arising from the stretched conformation of long overhangs as the total ssDNA length of 6R (36 nt) and 8R (48 nt) exceed the FRET sensitive distance range[39]. By contrast, when TRF2 was added to 6R and 8R pre-bound with POT1, we observed a sudden burst of FRET fluctuation which displays remarkably high FRET states up to 0.9 (Fig. 5a, b). Again, the appearance of high FRET emerged immediately after TRF2 addition, signifying the role of TRF2 in triggering the POT1-overhang looping dynamics. The heatmap generated by combining real-time traces (>50) reveals clearly the instantaneous spreading of FRET range concomitant with TRF2 binding (Fig. 5c, d). In the absence of TRF2, FRET range is more confined due to less molecules showing dynamics and less time spent in the dynamic state. The extremely high FRET of 0.9, despite the long length of overhang (6R, 8R) clearly indicates a completely looped configuration in which the 3' end of the POT1 bound overhang is recruited adjacent to TRF2 near the ds/ss junction.

To compare the POT1-overhang dynamics exhibited in the absence or presence of TRF2 in all four constructs, we collected FRET values from traces with representative FRET fluctuations in both conditions and plotted the range of FRET as heatmap histograms for 2R, 4R, 6R and 8R (Fig. 5e). While the FRET ranges observed in POT1 bound state vary as a function of telomeric overhang length, the TRF2 induced FRET fluctuation produced significantly greater variation in the FRET amplitude. For the shortest telomeric overhang, 2R which accommodates one POT1, the FRET range is similar with or without TRF2 due to the restricted movement in the short arm of the 12 nucleotide overhang (Fig. 5e, left top). For 4R, 6R and 8R overhang, the difference between POT1 without and with TRF2 become substantially more pronounced with the maximum difference exhibited by 8R in which the dynamic FRET range spans 0.1 to 0.9 (Fig. 5e, right bottom). Taken together, POT1 bound overhang is inherently dynamic and TRF2 bound *in cis* stimulates exceptionally dynamic loop formation by bringing the very end of 3' overhang to the telomere ds/ss junction repeatedly and persistently regardless of the length of the POT1 bound overhang (Fig. 5f).

Dynamic movement involves discrete steps

Upon a close examination of smFRET traces collected with POT1 and TRF2, we recognized that the FRET transitions between 0.1 and 0.9 were not smooth and continuous, but rather uneven and non-uniform (i.e there were discrete states which made the trace look jagged) (Supplementary Fig. 7). To check if there are discrete steps taken along the dynamic path, we employed an unbiased approach, termed hidden Markov Model (HMM) to analyse the dynamic smFRET traces. HMM analysis is ideal for identifying statistically significant distinct FRET levels within noisy smFRET traces[43]. The HMM algorithm was applied to fit smFRET traces obtained from POT1-TRF2 experiments performed with 4R, 6R, and 8R (Fig. 6a). For each construct, more than 50 dynamic traces were HMM fitted and the number of steps with their FRET values were extracted. All results of HMM analysis were combined to generate a transition density plot (TDP) for all three constructs[44]. TDP is a two-dimensional histogram plotted by taking FRET before transition on the x-axis and FRET after transition on the y-axis. Therefore, the ascending vs. descending FRET levels are populated on the upper left and lower right triangle coordinates, respectively. The interpretation is that

the ascending and descending steps represent looping and unlooping transitions, respectively. Since it's a density plot, the intensity of each spot indicates the visiting frequency at the given FRET state. The HMM analysis identified four distinct FRET states in TDP corresponding to four discrete steps of transitions embedded within the dynamic smFRET traces (Fig. 6b). Interestingly, the 4R, 6R, and 8R overhangs all showed the same pattern with highly similar FRET values (i.e ~0.35, ~0.55, ~0.7, and ~0.85 FRET states) (Fig. 6b). We note that some traces exhibit less than four states, yet the three, two and one steps of transitions all converge to the same four FRET states listed above, indicating well defined positions of contact between POT1-overhang complex and TRF2-duplex. The emerging picture is that POT1 is moving up and down the axis of the TRF2 bound telomeric duplex, undergoing differently looped states in a stepwise manner. The four distinct steps likely involve four units (two sets of homodimers) of TRF2 bound to telomeric duplex (Fig. 6c). Such movement is only observed when both POT1 and TRF2 are present (Supplementary Fig. 8a). Furthermore, the dwell times of the highest FRET (0.85) were highest in 8R ($\delta 2$ = ~8.2 sec), followed by 6R ($\delta 2$ = ~7.1 sec), and 4R ($\delta 2$ = ~3.2 sec), suggesting that the most highly looped state is more stabilized by the longer POT1 bound overhangs, likely due to less tension generated in looping longer POT1-overhang complex (Supplementary Fig. 8b). Interestingly, TRF2ΔB which lacks the basic domain, unlike TRF2, was not able to induce the highest FRET state evidenced by majority of smFRET traces displaying low to mid FRET dynamics devoid of the high FRET values of 0.7-0.9 (Supplementary Fig. 9). This indicates that TRF2ΔB cannot recruit the POT1 bound 3' end to the ds/ss-junction, consistent with the known function of basic domain in stabilizing the ds/ss three-way DNA junction[45].

To test if the number of FRET states correspond to the stoichiometry of TRF2, we reduced the valency of TRF2 to two (one homodimer) by shortening the length of the telomeric duplex to two TTAGGG repeats. Upon applying the same POT1 and TRF2 conditions, we indeed obtained two distinct FRET states (~0.55 and ~0.8) of dynamics from the HMM fitting of smFRET traces from 4R, 6R, and 8R overhangs (Fig. 6d). Subsequently, two discrete steps of transitions appeared on TDP analysis of all three constructs indicating a two ascending and two descending steps of movement taken by POT1-overhangs along the axis of TRF2-duplex (Fig. 6e). Hence, the discrete steps between the two proteins correspond to the distinct pairing between POT1 and TRF2 and the number of steps is proportional to the number of TRF2 homodimers on duplex (Fig. 6c, f).

TRF2 attenuates POT1 association

So far, POT1 was added prior to TRF2. Next, we asked if the TRF2 bound state impacts POT1 binding by applying POT1 after TRF2 (Fig. 7a). The TRF2 (25 nM) binding to telomeric duplex did not change the FRET peak (at ~0.65) as before (Fig. 7b). When POT1 (50 nM) was added, the FRET peak displayed an extremely delayed shift to low FRET (~0.3) indicating an inefficient binding of POT1. Unlike the few seconds that POT1 takes to bind an overhang with unbound duplex (Fig. 1), it took 3 minutes to observe ~50% binding and 20 minutes to reach ~90% bound fraction (Fig. 7b). For kinetics analysis, the bound fractions (0.3 FRET peak) of POT1 alone and TRF2 followed by POT1 collected over time and fitted to exponential decay to obtain the rate of binding (Fig. 7c). The same experiment performed with a non-

telomeric duplex, where no TRF2 is expected to bind, revealed the same POT1 binding rate (Supplementary Fig. 10). Hence, this clearly demonstrates that the presence of TRF2 at the duplex interferes with and delays the POT1 binding to the telomeric overhang.

Next, we asked if the delayed binding is due to TRF2 interacting with the G4 structure formed at the overhang. We reasoned that TRF2 as a key factor at the ds/ss junction of telomere may be contacting the overhang structure although it does not change the conformation of the overhang (Fig. 7b). To test this effect, we applied the same sequence of TRF2 followed by POT1, to 2R and 3R, which don't form higher order structures, and to 6R and 8R, which can form G4 structures[42]. First, we compared the rate of POT1 binding and found that the rate decreases as a function of overhang length (Fig. 7d, orange bars). In the presence of TRF2 bound at the duplex, the POT1 binding rate to 2R and 3R were comparable to the case of POT1 only (Fig. 7d, blue bars). By contrast, it displayed a marked decrease in 4R, 6R, and 8R, suggesting that the TRF2-duplex interacts with the structured telomeric overhang and thereby, attenuates and delays the POT1 binding (Fig. 7d, blue bars). Interestingly, when POT1 and TRF2 were added simultaneously to all constructs (2R to 8R), we found a similar delayed POT1 binding for 4R, 6R and 8R (Fig. 7d), consistent with the higher binding rate of TRF2-duplex (~4-fold) than POT1-overhang (Supplementary Fig. 5). The cellular POT1 concentration is about ~5-10-fold lower than TRF2 and the K_D of POT1 is higher than TRF2[9,13], raising the possibility of this scenario. However, further experiment is warranted to test the order of binding in the presence of other shelterin proteins.

Discussion

In this work, we report an unanticipated dynamic nature of the POT1-overhang complex which makes frequent contact with the duplex, suggesting an inherent bendability or flexibility of the structure. Remarkably, such conformational dynamics of the POT1-overhang is dramatically increased by TRF2 bound at the telomeric duplex *in cis*. Intriguingly, the movement is systematically coordinated by the two proteins, evidenced by the discrete stepwise FRET changes we monitored only in the presence of both POT1 and TRF2. The number of steps correspond to the number of TRF2 homodimers bound to the duplex and the same steps persist regardless of the length of the POT1 bound overhang. Based on this result, we propose a dynamic looping mechanism by which TRF2 actively recruits the tip of the POT1-overhang and enables a stepwise movement up and down the axis of telomeric duplex. This intrinsic mobility may continue until stabilized or linked by other shelterin components, thus providing a flexible platform for establishing a t-loop at a desired location and context (Fig. 8).

Telomere end-binding protein POT1 disrupts the G4 in a stepwise manner, one OB-fold at a time, and thereby resulting in a highly stable complex (Fig. 1)[23,24]. Unlike other ssDNA binding proteins, such as SSB, RecA and Rad51, POT1 binds telomeric overhang with an exquisite sequence specificity and produces a sharp kink[23,24,46-48]. Despite the highly stable binding, POT1 induced telomeric overhang dynamics even at monomer bound states (Fig. 3). The POT1 induced telomeric overhang dynamics is uniquely distinguished from other classes of ssDNA binding proteins including RPA which diffuses along

ssDNA[49] as well as RecA and Rad51 which form a stable helical filament and undergo ATP dependent dynamic assembly and disassembly[46-48]. The pattern of FRET fluctuations induced by POT1 bound to G4 overhangs suggests transient and dynamic loop formation (Fig. 2). The fast transition to high FRET seen in Dynamic-II may represents a rotation of the 3' terminal POT1 around the other unit, using the two guanine spacer as a pivot point (Fig. 2), bringing the 3' end near the ds/ss junction. The POT1 binding to overhangs linked to telomeric vs. non-telomeric duplexes yielded the same result, indicating that the transient looping activity is an intrinsic property of the POT1-overhang complex, independent of the duplex sequence.

Our results revealed an intriguing property of TRF2 in recruiting the POT1-overhang and inducing a stepwise movement up and down the telomeric duplex axis without requiring an external source of energy (Fig. 4). This is reminiscent of the t-loop/D-loop that forms in the context of telomeric duplex where the overhang invades by assistance of shelterin components[9,32]. The emerging picture based on the FRET fluctuation pattern is that the tip of the POT1-overhang complex makes physical contact with each homodimer of TRF2 bound on duplex, rendering four steps corresponding to four TRF2 or two steps for two TRF2 units. This motion is transient, dynamic, yet persistent, giving rise to dynamic looping where the looped circle undergoes tightening and expanding continuously. Such movement requires that both TRF2 and POT1 proteins interact with the telomeric duplex and overhang, respectively as TRF2 applied *in-trans* to non-telomeric duplex cannot recapitulate the dynamic looping activity. One plausible scenario is that such dynamic motion is used for assembling shelterin in which POT1 and TRF2 need to be linked to adjacent proteins including TPP1, RAP1, TRF1 and TIN2[9,10]. Consistently, previous report suggested that TRF2 uses one-dimensional sliding to find the partner proteins and assemble into the shelterin complex[13,34]. Further, POT1 and TRF2 may interact with each other to form a complex with telomeric DNA[35] and, POT1 are TRF2 are co-localized within a larger complex at the telomere[12,50]. POT1 and TRF2 cooperate to maintain the telomeric length and POT1 helps to stabilize the t-loop generated by TRF2 to protect the telomere end[9,35]. Our study adds to the previous findings by demonstrating that TRF2 and POT1, upon binding the telomeric duplex and overhang, respectively, generate a highly dynamic looping motion with discrete steps which may lead to finding a correct t-loop configuration assisted by other shelterin components (Fig. 8). Our observations with the TRF2ΔB mutant is in agreement with the previous finding that TRF2, but not TRF2ΔB binds branched DNA to protect three- and four-way junction during t-loop formation[45,51]. In addition, our result suggests a role of TRF2 basic domain in recruiting the POT1 bound 3' end to the telomeric junction and thereby forming a proper t-loop conformation (Fig. 8).

What is the driving force of the stepwise movement? There are three possible contributing aspects. First, the complementarity between the overhang and the C-rich strand in duplex can generate base pairing, but this alone does not explain the continuous transitions from one state to another. Second, POT1 can induce dynamic bending of overhang as shown, yet POT1 alone produced dynamic patterns (Dynamic-I, -II) which differed from the four steps observed in the presence of TRF2. Third, TRF2 can recruit the overhang strand to stimulate invasion, but TRF2 without POT1 did not produce any FRET change, which led us to use PIFE to probe its association (Supplementary Fig. 5). It is clear from our observations that

both POT1 and TRF2 positioned in the overhang and duplex of telomere, respectively, are required for this looping activity. The base pairing may play a role, but only in the context of both proteins engaged with the DNA. We note that amongst the five FRET states that constitutes the four steps, the lowest FRET value corresponds to the POT1 bound extended overhang without engaging with TRF2. Therefore, the dynamic motion includes excursions to the un-looped state interspersed with the differently looped states.

One of the most surprising conformations was revealed by the extremely high FRET (~0.9) state observed in DNA with a long overhang such as 6R and 8R (i.e 36-48 nucleotides). POT1 alone induced mostly low FRET states which agrees with the tandemly bound POT1 along the overhang. However, in the presence of both POT1 and TRF2, the FRET level rose to 0.9, clearly indicating a loop which forms by bringing the 3’ end to ss/ds junction (Fig. 5e). This is consistent with the telomere capping model in which the 3’ end of the telomere loops to invade the duplex to form the t-loop[32]. In addition, the shelterin complex is positioned near the 3’ end where TPP1 and POT1 regulate telomerase recruitment to the 3’ end[52,53]. POT1 has a higher affinity to the 3’ end sequence TTAG, to stabilize the shelterin complex[54]. Hence the 3’ end is the key moiety of telomeric overhang which plays a critical role in shelterin maintenance, t-loop formation and telomerase recruitment.

TRF2 was shown to be necessary and sufficient for t-loop formation but the exact invading mechanism of the 3’ overhang into the telomeric duplex remains elusive[9,29]. In agreement with our result, TRF2 only bound to telomeric duplex, but not the single stranded overhang[19]. TRF2 may remodel telomeric DNA into t-loop by wrapping the DNA using TRFH domain which induces local unwinding and invasion by the 3’ overhang[55]. The discrepancy in our study may be due to the limited length of the overhangs or TRF2 concentration. When t-loops from HeLa cells were incubated with *E. coli* single-stranded binding protein (SSB), SSB bound primarily at the t-loop junction[32]. Similarly, POT1 positions at the t-loop junction, which is critical for the invasion activity[9,19,32]. Our finding of the dynamic loop formation mechanism may represent the intermediate stages that can scan for the desired t-loop position along the telomeric duplex.

T-loops can have a long duplex with a short overhang tail or vice versa[1,31]. But the exact structure of the t-loop and the minimal length of telomere required for t-loop formation are not known[1,9]. Our construct with 24 base pairs of telomeric duplex and up to 48 nucleotides of overhang did not lead to a stable loop. Nevertheless, the longer dwell times at the high FRET state displayed by the longer overhang 6R and 8R may indicate a higher stability of overhang association with the duplex (Supplementary Fig. 8). Perhaps there is a length requirement for the POT1-overhang to stably associate and invade into duplex to form a t-loop. It can also be due to the internal strain caused by the short loop that prevented a stable loop formation. Additionally, the duplex length and limited binding of TRF2 may have limited the overhang invasion. The t-loop formation can take two possible routes; first, 3’ end invades a particular region of duplex from which loop propagates to the 5’ end, thus making a long D-loop; second, 3’ end invades and moves forward without expanding the D-loop length. Our observation of 3’ end stepping up and down can

support both mechanisms of invasion although the latter model is more fitting since the extensive D-loop may slow down the mobility due to the higher thermal stability of the triplex.

Interestingly, we found that POT1 binding was significantly delayed in the presence of TRF2 in the duplex. The delay was only observed at 4R, 6R and 8R but not at 2R and 3R (Fig. 7). TRF2 preferentially binds the ds/ss junction of telomeres, near the POT1 binding site[10,31]. Therefore, TRF2 may have a natural binding affinity to G4 or G4 containing higher ordered structure to attenuate POT1 binding. Indeed, our kinetic analysis revealed that the binding rate of the TRF2-duplex is ~ 4 times fast than the POT1-overhang, which makes TRF2 associate before POT1 binding (Supplementary Fig. 5). Further, the cellular POT1 concentration is about ~5–10-fold lower than TRF2, and the K_D of POT1 is higher than TRF2[9,13], raising the possibility of this scenario. Nevertheless, further experiment is warranted to test the order of binding in the presence of other shelterin proteins.

One important function of shelterin is to protect telomeres from unwanted degradation and end-to-end fusion[1,2]. Shelterin complex harbouring both TRF2 and POT1 plays a pivotal role in end protection by preventing activation of the ATM and ATR kinase DNA damage response[14,45]. Evidence suggests that POT1 and TRF2 search for telomeric ss/ds junctions by three-dimensional diffusion and upon binding, POT1 scans along the ss-overhang to stabilize the 3’ end (Fig. 8d)[10,13,34]. The mobile property generated by POT1 and TRF2 that we report here may contribute to the mechanism of shelterin assembly, telomere protection and telomerase recruitment.

Methods

Preparation of DNA constructs

The HPLC purified biotin and Cy3/Cy5 labeled oligonucleotides used for immobilization and for FRET measurements respectively, were purchased from IDT (tabulated in Supplementary Table 1). Each of the partial duplex DNA constructs (10 μM) were prepared by mixing biotin-conjugated DNA strand with its complementary strand at a molar ratio of 1:1.2 (biotinylated : non-biotinylated). They were annealed in T50 buffer (10 mM Tris–HCl, pH 7.5 and 50 mM NaCl) on a thermocycler by heating to 95 °C for 2 min, then gradually cooling at the rate of 2 °C/min until they reached 40 °C, followed by further 5 °C/min cooling until they reached 4 °C. Telomeric duplex (i.e. two and four repeat of TTAGGG duplex with overhangs) were annealed in 10 mM Tris–HCl, pH 7.5 and 5 mM $MgCl_2$ containing buffer following the same protocol as described above. Milli-Q water was used to prepare all buffers and then filtered through 0.22 μm membrane filters.

Protein purification

Recombinant human POT1 protein was expressed in a baculovirus/insect cell system and was purified as previously described[23,56]. TRF2 expression plasmids were transformed into BL21 (DE3) competent *E. coli* cells (NEB). Cells were cultured at 37 °C till OD 600 reached 0.4 and then TRF2 expression was

induced with 50 μM IPTG. Proteins were expressed at 25 °C for 5 hours. Harvested cell pellets were lysed by sonication in 25 ml of lysis buffer (50 mM Tris-HCl, 0.6 M NaCl, 10% glycerol, 1% Tween 20, 3 mM b-mercaptoethanol, 1% NP-40, Protease inhibitor tablet and 1 mM PMSF, pH 7), followed by centrifugation at 20,000 g for 1 hour at 4 °C. TRF2 was purified using GST-Affinity columns. The supernatant was passed through a GSTrap^{TM} HP column (GE), using an AKTA pure 25 M FPLC system (GE), in the buffer (50 mM sodium phosphate, 100 mM NaCl and 5 mM b-mercaptoethanol, pH 7). Proteins were eluted using the elution buffer (50 mM sodium phosphate, 100 mM NaCl, 5 mM b-mercaptoethanol and 25 mM reduced glutathione, pH 7). Fractions that collected TRF2 were pooled and stored in 5-10% Glycerol at -80 °C.

Slide surface preparation

For all the single-molecule experiments passivated PEG slides were used to avoid any non-specific interactions of excess DNA or protein. Generally, predrilled quartz slides and glass coverslips were thoroughly washed with methanol, acetone and etched by sonication in 1 M potassium hydroxide. Then, slides were burned for 2-3 minutes, and coverslips were quickly sterilized by passing through the flame 4-5 times to remove all sources of fluorescence. Subsequently, the slides and coverslips were coated with aminosilane for 30-45 minutes, then treated with a mixture of 98% mPEG (m-PEG-5000, Laysan Bio, Inc.) and 2% biotin PEG (biotin-PEG-5000, Laysan Bio, Inc) over night. The slides and coverslips were then washed and dried using nitrogen gas and stored in −20 °C for future experiments. Finally, the microfluidic sample chamber was created between the plasma cleaned slide and the coverslip was coated with PEG and biotin-PEG.

Single-molecule FRET and PIFE measurements

A custom built prism-type total internal reflection (PTIR) inverted fluorescence microscope (Olympus IX 71) was used for single-molecule FRET (smFRET) measurements as described earlier[48,57]. Freshly annealed stock partial duplex DNA labeled with biotin, Cy3, and Cy5 were diluted to 15-20 pM in the buffer of 10 mM Tris-HCl, pH 7.5 and 100 mM NaCl. The diluted DNA was immobilized on the PEG-passivated surface via biotin–neutravidin (50 μg/ml) linkage and unbound molecules were washed using the same buffer. All the smFRET measurements were carried out in an imaging buffer containing 10 mM Tris-HCl, pH 7.5, 100 mM NaCl, 10% glycerol with an oxygen scavenging system (10 mM trolox, 0.5% glucose, 1 mg/ml glucose oxidase and 4 μg/ml catalase) to avoid blinking and to improve dyes stability. All smFRET assays were performed at room temperature (~ 23 °C ± 2 °C). Similar procedures were followed for real-time PIFE (protein induced fluorescence enhancement) measurements using either green or red laser.

Data Acquisition

The evanescent field was generated through PTIR using a solid state of either 532 or 634 nm diode laser (Compass 315M, Coherent) to excite the fluorophores (Cy3 or Cy5) at the sample chamber. The fluorescence from the fluorophores (Cy3 (donor) and Cy5 (acceptor)) were simultaneously collected using

water immersion objective. A dichroic mirror (cut off = 630 nm) was used to separate the emission signals and finally projected them onto an EMCCD camera (Andor). Data was recorded with 100 ms frame integration time, then processed by IDL script, and finally analyzed by Matlab scripts.

smFRET data analysis

FRET histograms were generated from more than 4000 molecules (21 frames of 20 short movies) collected from different imaging surfaces. To exclude the donor only molecules from the histogram at the low FRET region, green and red lasers were sequentially used to excite Cy3 and Cy5 respectively (10 frames for Cy3, 1 frame dark and 10 frames for Cy5). Additionally, the donor-leakage was corrected based on the FRET values of donor-only molecules. The histograms were normalized and fitted to Gaussian distributions in Origin 2018 with unrestrained peak center position. Matlab code was used to measure the dwell time and then single exponentially fitted in Origin 2018 to extract decay time. The FRET heatmaps were generated by an in-house MATLAB script overlaying more than 100 traces. HaMMy fitting of single-molecule time traces and transition density plots (TDP) were generated by using the free software available from the website https://cplc.illinois.edu/software/. To find out the certain number of distinct FRET states of our given system, we HaMMy fitted individually the dynamic smFRET traces of all different constructs. We applied more than the number of expected FRET states i.e. six or eight states for HaMMy fitting. HaMMy determine the most likely combination of FRET states and the corresponding transition rate i.e. state-to-state transition probabilities[43,47]. Finally the transition density plot (TDP) was generated by using HaMMy fitted the number of each transition and irrespective of given six or eight number of different states, TDP looks almost identical.

smFRET real-time experiment

The smFRET real-time POT1 binding to G4/R4 and TRF2 binding to telomeric duplex assays were carried out with a micro-fluidic imaging flow chamber. A small piece of the plastic reservoir was placed above the one hole at one end of the chamber and corresponding other holes at the opposite end was connected to a silicone tube with a syringe pump (Harvard Apparatus, MA). Either POT1 or TRF2 suspended in imaging buffer was loaded into the reservoir. The real-time FRET images were collected by passing solution through the imaging chamber via silicone tubing at a flow rate of 20 µL/s. The smFRET time trajectories were analyzed using Matlab scripts. Using the individual single-molecule real-time flow traces, FRET flow heatmaps were generated. POT1 binding kinetics were calculated from the moment of flow to the moment of first irreversible FRET decline. In each case more than 100 molecules were incorporated.

Declarations

Acknowledgements

We thank to Dr. Hui-Ting Lee and Dr. Amirhossein Ghanbari Niaki **for** help in developing the MatLab script used for data analysis and heatmap preparation. We thank to Dr. Taekjip Ha for helpful discussion and the members of the Sua Myong and Taekjip Ha laboratory for helpful comments. We thank to Dr. Claus

Maria Azzalin for the gift of TRF2 plasmid. This work was supported by the National Institute of Health General Medicine (1R01GM115631-01A1) to T.P. and S.M., National Science Foundation Physics Frontiers Center Program (0822613) through the Center for the Physics of Living Cells to S.M., NCI (R01CA207341) to S.M and P.L.O. and NIEHS R35ES030396 to P.L.O.

Author contributions

T.P. and S.M. designed and planned the research; T.P. performed all experiments with the assistance provided by W.L. and X.C; T.P. and S.M. analysed the data; and T.P. and S.M. wrote the manuscript and P.L.O. and W.L. edited the manuscript. P.L.O provided purified proteins. All authors have given approval to the final version of the manuscript.

Competing interest

The authors declare no competing financial interests.

References

1. De Lange, T. Shelterin: the protein complex that shapes and safeguards human telomeres. *Genes & development* **19**, 2100-2110 (2005).
2. Sfeir, A. & De Lange, T. Removal of shelterin reveals the telomere end-protection problem. *Science* **336**, 593-597 (2012).
3. Bandaria, J.N., Qin, P., Berk, V., Chu, S. & Yildiz, A. Shelterin protects chromosome ends by compacting telomeric chromatin. *Cell* **164**, 735-746 (2016).
4. Farr, C., Fantes, J., Goodfellow, P. & Cooke, H. Functional reintroduction of human telomeres into mammalian cells. *Proceedings of the National Academy of Sciences* **88**, 7006-7010 (1991).
5. Reddel, R.R. Alternative lengthening of telomeres, telomerase, and cancer. *Cancer letters* **194**, 155-162 (2003).
6. Makarov, V.L., Hirose, Y. & Langmore, J.P. Long G tails at both ends of human chromosomes suggest a C strand degradation mechanism for telomere shortening. *Cell* **88**, 657-666 (1997).
7. Blackburn, E.H. Telomere states and cell fates. *Nature* **408**, 53 (2000).
8. Palm, W. & de Lange, T. How shelterin protects mammalian telomeres. *Annual review of genetics* **42**, 301-334 (2008).
9. de Lange, T. Shelterin-mediated telomere protection. *Annual review of genetics* **52**, 223-247 (2018).
10. Lim, C.J., Zaug, A.J., Kim, H.J. & Cech, T.R. Reconstitution of human shelterin complexes reveals unexpected stoichiometry and dual pathways to enhance telomerase processivity. *Nature communications* **8**, 1-14 (2017).

11. Ye, J.Z.-S. et al. TIN2 binds TRF1 and TRF2 simultaneously and stabilizes the TRF2 complex on telomeres. *Journal of Biological Chemistry* **279**, 47264-47271 (2004).
12. Liu, D., O'Connor, M.S., Qin, J. & Songyang, Z. Telosome, a mammalian telomere-associated complex formed by multiple telomeric proteins. *Journal of Biological Chemistry* **279**, 51338-51342 (2004).
13. Erdel, F. et al. Telomere recognition and assembly mechanism of mammalian shelterin. *Cell reports* **18**, 41-53 (2017).
14. Denchi, E.L. & de Lange, T. Protection of telomeres through independent control of ATM and ATR by TRF2 and POT1. *Nature* **448**, 1068-1071 (2007).
15. Karlseder, J., Broccoli, D., Dai, Y., Hardy, S. & de Lange, T. p53-and ATM-dependent apoptosis induced by telomeres lacking TRF2. *Science* **283**, 1321-1325 (1999).
16. Cech, T.R. Beginning to understand the end of the chromosome. *Cell* **116**, 273-279 (2004).
17. Cesare, A.J., Hayashi, M.T., Crabbe, L. & Karlseder, J. The telomere deprotection response is functionally distinct from the genomic DNA damage response. *Molecular cell* **51**, 141-155 (2013).
18. Xin, H., Liu, D. & Songyang, Z. The telosome/shelterin complex and its functions. *Genome biology* **9**, 232 (2008).
19. De Lange, T. T-loops and the origin of telomeres. *Nature reviews Molecular cell biology* **5**, 323-329 (2004).
20. Stewart, S.A. et al. Erosion of the telomeric single-strand overhang at replicative senescence. *Nature genetics* **33**, 492-496 (2003).
21. Baumann, P. & Cech, T.R. Pot1, the putative telomere end-binding protein in fission yeast and humans. *Science* **292**, 1171-1175 (2001).
22. Lei, M., Podell, E.R., Baumann, P. & Cech, T.R. DNA self-recognition in the structure of Pot1 bound to telomeric single-stranded DNA. *Nature* **426**, 198-203 (2003).
23. Lei, M., Podell, E.R. & Cech, T.R. Structure of human POT1 bound to telomeric single-stranded DNA provides a model for chromosome end-protection. *Nature structural & molecular biology* **11**, 1223-1229 (2004).
24. Hwang, H., Buncher, N., Opresko, P.L. & Myong, S. POT1-TPP1 regulates telomeric overhang structural dynamics. *Structure* **20**, 1872-1880 (2012).
25. Ray, S., Bandaria, J.N., Qureshi, M.H., Yildiz, A. & Balci, H. G-quadruplex formation in telomeres enhances POT1/TPP1 protection against RPA binding. *Proceedings of the National Academy of Sciences* **111**, 2990-2995 (2014).
26. Lee, H.-T. et al. Position-Dependent Effect of Guanine Base Damage and Mutations on Telomeric G-Quadruplex and Telomerase Extension. *Biochemistry* **59**, 2627-2639 (2020).
27. Taylor, D.J., Podell, E.R., Taatjes, D.J. & Cech, T.R. Multiple POT1–TPP1 proteins coat and compact long telomeric single-stranded DNA. *Journal of molecular biology* **410**, 10-17 (2011).
28. Takai, K.K., Hooper, S., Blackwood, S., Gandhi, R. & de Lange, T. In vivo stoichiometry of shelterin components. *J Biol Chem* **285**, 1457-67 (2010).

29. Doksani, Y., Wu, J.Y., de Lange, T. & Zhuang, X. Super-resolution fluorescence imaging of telomeres reveals TRF2-dependent T-loop formation. *Cell* **155**, 345-356 (2013).
30. Doksani, Y. & de Lange, T. The role of double-strand break repair pathways at functional and dysfunctional telomeres. *Cold Spring Harbor perspectives in biology* **6**, a016576 (2014).
31. Stansel, R.M., de Lange, T. & Griffith, J.D. T-loop assembly in vitro involves binding of TRF2 near the 3' telomeric overhang. *The EMBO journal* **20**, 5532-5540 (2001).
32. Griffith, J.D. et al. Mammalian telomeres end in a large duplex loop. *Cell* **97**, 503-514 (1999).
33. Van Ly, D. et al. Telomere loop dynamics in chromosome end protection. *Molecular cell* **71**, 510-525. e6 (2018).
34. Lin, J. et al. TRF1 and TRF2 use different mechanisms to find telomeric DNA but share a novel mechanism to search for protein partners at telomeres. *Nucleic acids research* **42**, 2493-2504 (2014).
35. Yang, Q., Zheng, Y.-L. & Harris, C.C. POT1 and TRF2 cooperate to maintain telomeric integrity. *Molecular and cellular biology* **25**, 1070-1080 (2005).
36. Kendellen, M.F., Barrientos, K.S. & Counter, C.M. POT1 association with TRF2 regulates telomere length. *Mol Cell Biol* **29**, 5611-9 (2009).
37. Timashev, L.A. & De Lange, T. Characterization of t-loop formation by TRF2. *Nucleus* **11**, 164-177 (2020).
38. Lee, H.-T., Bose, A., Lee, C.-Y., Opresko, P.L. & Myong, S. Molecular mechanisms by which oxidative DNA damage promotes telomerase activity. *Nucleic acids research* **45**, 11752-11765 (2017).
39. Murphy, M., Rasnik, I., Cheng, W., Lohman, T.M. & Ha, T. Probing single-stranded DNA conformational flexibility using fluorescence spectroscopy. *Biophysical journal* **86**, 2530-2537 (2004).
40. Hwang, H., Kim, H. & Myong, S. Protein induced fluorescence enhancement as a single molecule assay with short distance sensitivity. *Proceedings of the National Academy of Sciences* **108**, 7414-7418 (2011).
41. Hwang, H. & Myong, S. Protein induced fluorescence enhancement (PIFE) for probing protein–nucleic acid interactions. *Chemical Society reviews* **43**, 1221-1229 (2014).
42. Hwang, H. et al. Telomeric overhang length determines structural dynamics and accessibility to telomerase and ALT-associated proteins. *Structure* **22**, 842-853 (2014).
43. McKinney, S.A., Joo, C. & Ha, T. Analysis of single-molecule FRET trajectories using hidden Markov modeling. *Biophysical journal* **91**, 1941-1951 (2006).
44. Tippana, R., Chen, M.C., Demeshkina, N.A., Ferré-D'Amaré, A.R. & Myong, S. RNA G-quadruplex is resolved by repetitive and ATP-dependent mechanism of DHX36. *Nature communications* **10**, 1-10 (2019).
45. Schmutz, I., Timashev, L., Xie, W., Patel, D.J. & de Lange, T. TRF2 binds branched DNA to safeguard telomere integrity. *Nature structural & molecular biology* **24**, 734 (2017).
46. Qiu, Y. et al. Srs2 prevents Rad51 filament formation by repetitive motion on DNA. *Nature communications* **4**, 1-10 (2013).

47. Joo, C. et al. Real-time observation of RecA filament dynamics with single monomer resolution. *Cell* **126**, 515-527 (2006).
48. Paul, T. et al. E. coli Rep helicase and RecA recombinase unwind G4 DNA and are important for resistance to G4-stabilizing ligands. *Nucleic Acids Research* (2020).
49. Ma, C.J., Gibb, B., Kwon, Y., Sung, P. & Greene, E.C. Protein dynamics of human RPA and RAD51 on ssDNA during assembly and disassembly of the RAD51 filament. *Nucleic acids research* **45**, 749-761 (2017).
50. O'Connor, M.S., Safari, A., Xin, H., Liu, D. & Songyang, Z. A critical role for TPP1 and TIN2 interaction in high-order telomeric complex assembly. *Proceedings of the National Academy of Sciences* **103**, 11874-11879 (2006).
51. Nora, G.J., Buncher, N.A. & Opresko, P.L. Telomeric protein TRF2 protects Holliday junctions with telomeric arms from displacement by the Werner syndrome helicase. *Nucleic acids research* **38**, 3984-3998 (2010).
52. Abreu, E. et al. TIN2-tethered TPP1 recruits human telomerase to telomeres in vivo. *Molecular and cellular biology* **30**, 2971-2982 (2010).
53. Laprade, H. et al. Single-molecule imaging of telomerase RNA reveals a Recruitment-Retention model for telomere elongation. *Molecular Cell* (2020).
54. Sfeir, A.J., Chai, W., Shay, J.W. & Wright, W.E. Telomere-end processing: the terminal nucleotidesof human chromosomes. *Molecular cell* **18**, 131-138 (2005).
55. Benarroch-Popivker, D. et al. TRF2-mediated control of telomere DNA topology as a mechanism for chromosome-end protection. *Molecular cell* **61**, 274-286 (2016).
56. Sowd, G., Lei, M. & Opresko, P.L. Mechanism and substrate specificity of telomeric protein POT1 stimulation of the Werner syndrome helicase. *Nucleic acids research* **36**, 4242-4256 (2008).
57. Paul, T., Bera, S.C. & Mishra, P.P. Direct observation of breathing dynamics at the mismatch induced DNA bubble with nanometre accuracy: a smFRET study. *Nanoscale* **9**, 5835-5842 (2017).

Figures

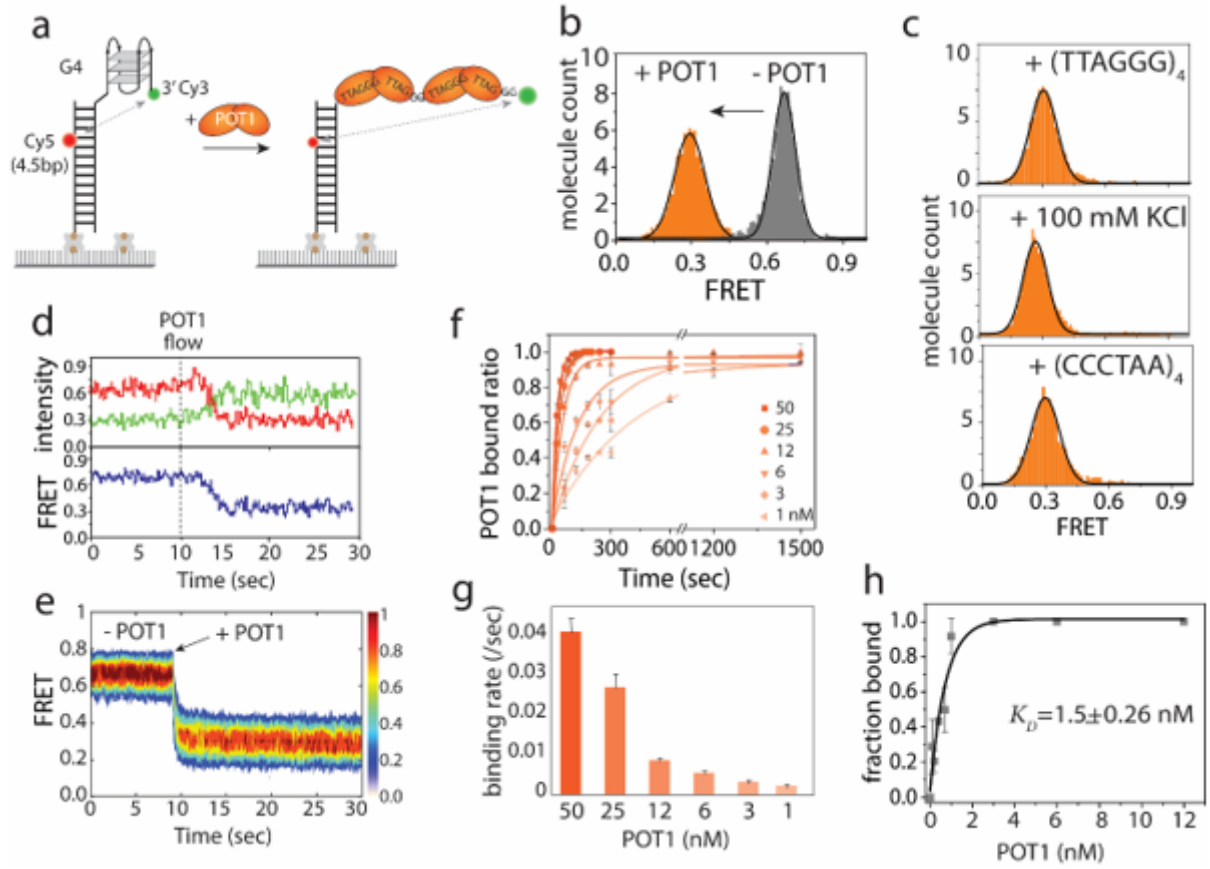

Figure 1

POT1 is stably bound to telomeric G4/4R. a, Schematic smFRET model of before and after POT1 binding to telomeric G4/4R DNA (Top4.5 construct). b, The FRET histograms of 4R before and after POT1 binding. c, FRET histograms after 30 minutes incubation with 4R only (top), 100 mM KCl (center) and C4 (bottom) to the POT1 bound G4. d, The representative real-time smFRET trace of POT1 binding to 4R (protein flow at ~10 sec). e, The heatmap (n>100), generated by synchronizing the POT1 bound state. f, Single-exponential fitting of POT1 bound fraction to 4R at different concentrations. g, The bar graph represents the corresponding POT1 binding rate. h, Determination of the dissociation constant (KD) of POT1 to 4R/G4.

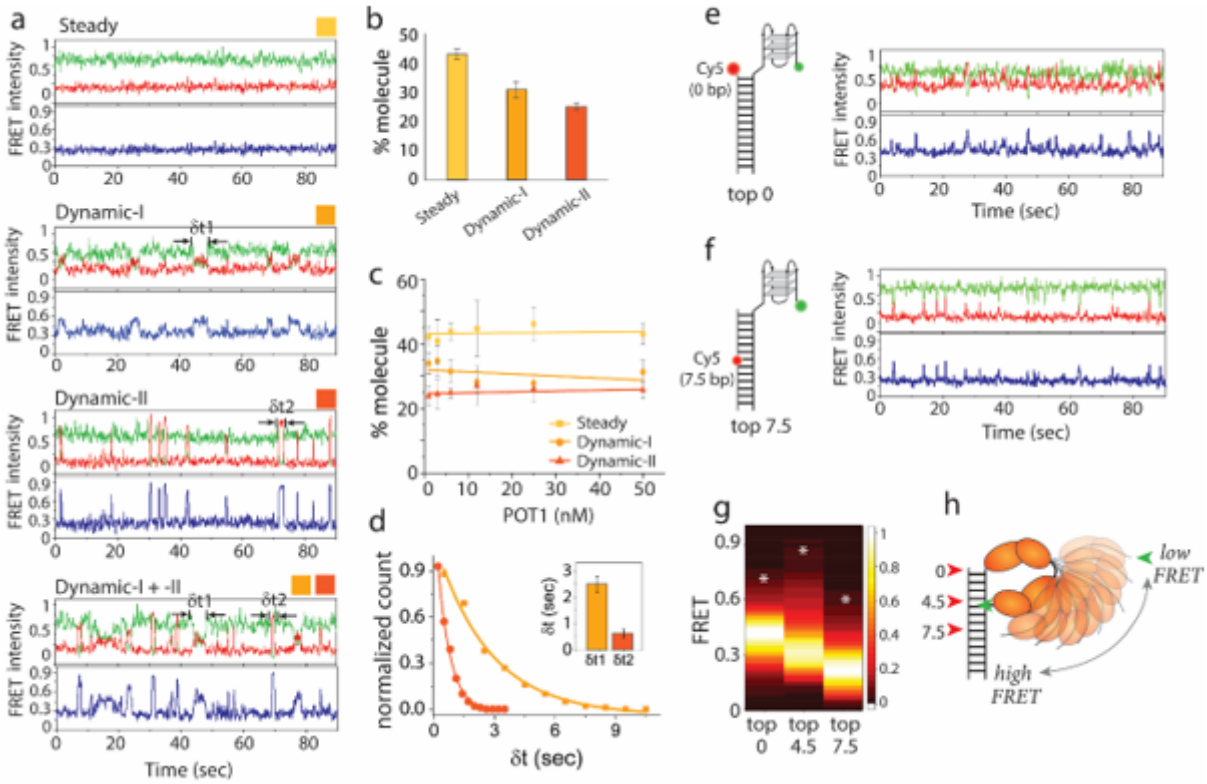

Figure 2

POT1 bound telomeric overhang shows dynamics. a, The representative smFRET traces of POT1 bound to telomeric 4R after wash of free protein show steady (FRET ~0.3, top), Dynamic-I (FRET ~0.2-0.6, second from top), and Dynamic-II (FRET ~0.2-0.9, bottom two) traces. (b & c), Quantification of molecular behavior of POT1 bound G4 (steady vs. two types of dynamic) at 25 nM after wash of free protein (b) and the protein concentrations ranging from 50 nM to 1 nM before wash of free protein (c). d, Dwell time of dynamic FRET traces, δt1 for dynamic-I and δt2 for dynamic–II respectively. (e & f), Model cartoon of Top0 (e) and Top7.5 (f) 4R construct, based on the acceptor dye position from the top of the duplex and the representative POT1 bound smFRET traces respectively. g, FRET heatmap histogram of three constructs generated from the dynamic traces. White asterisk denote level of highest FRET values observed in traces. h, Schematic dynamic model of POT1 bound telomeric G4 overhang.

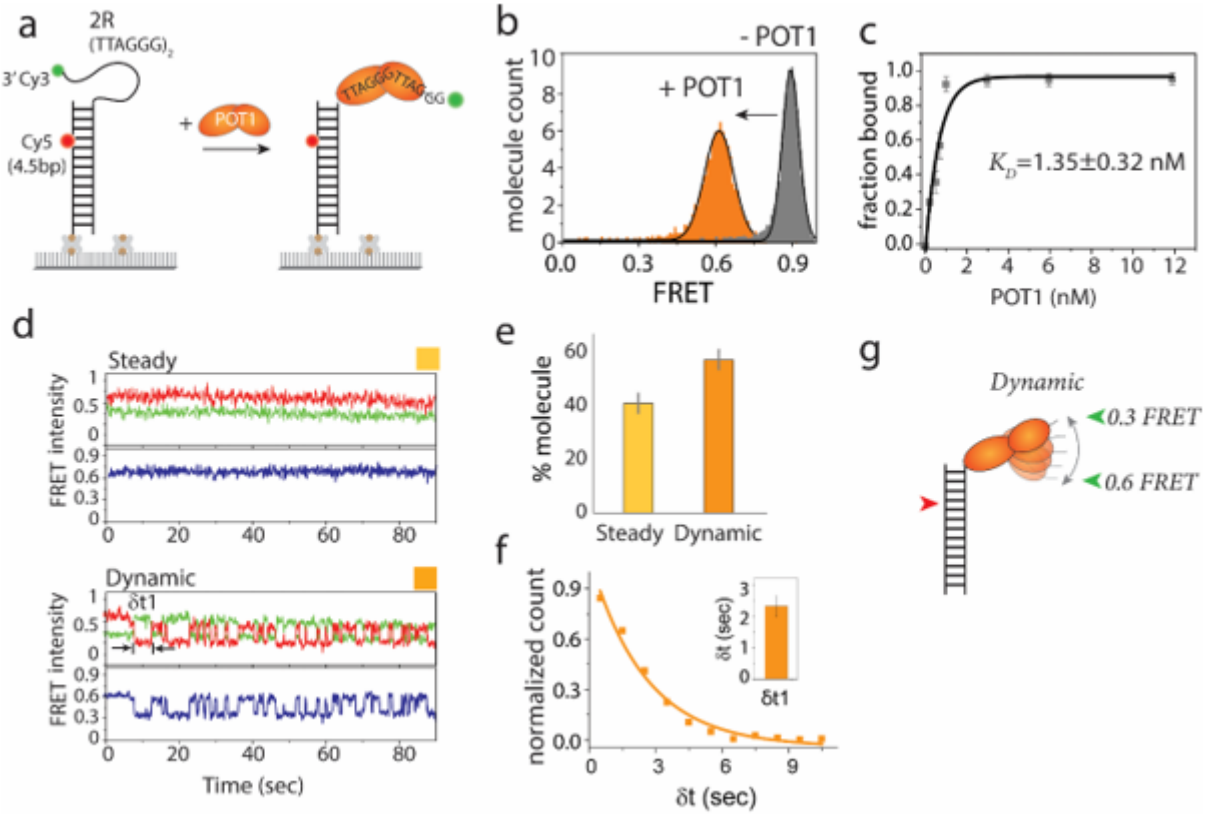

Figure 3

Monomer POT1 bound telomeric overhang shows dynamics. a, Schematic smFRET model cartoon before and after POT1 binding to the telomeric 2R overhang where the acceptor dye (red) is labeled at top4.5 position. b, The FRET histograms of 2R before and after POT1 binding. c, Determination of the dissociation constant (KD) of POT1 to 2R. d, The representative smFRET steady (top) and dynamic (bottom) traces of POT1 bound to telomeric 2R. e, Quantification of molecular behavior of POT1 bound 2R (steady vs dynamic). f, Dwell time (δt1) of dynamic FRET traces. g, Schematic dynamic model of POT1 bound telomeric 2R overhang.

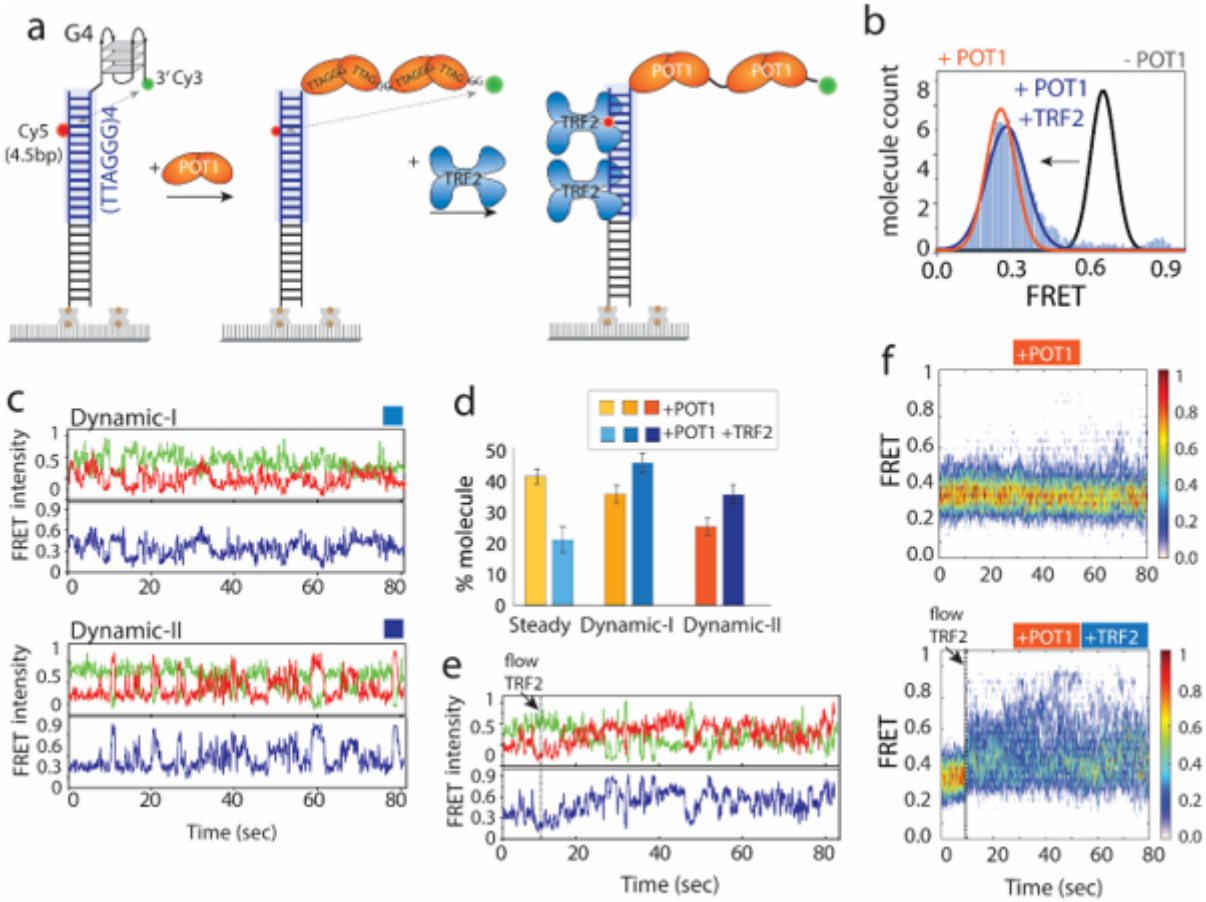

Figure 4

Telomeric duplex bound TRF2 enhances POT1-overhang dynamics. a, Schematic model of telomeric duplex (four repeats of TTAGGG tract) with G4 overhang sequentially binding POT1 at the overhang followed by TRF2 at the duplex. b, The FRET histograms of telomeric duplex with G4 (~0.65 FRET, black solid line), POT1 bound condition (~0.3 FRET, orange solid line), and POT1, TRF2 together (~0.3 FRET, solid blue filled). c, POT1 and TRF2 bound representative smFRET traces of Dynamic-I (top) and Dynamic-II (bottom) states. d, Quantification of molecular behaviour (steady vs two types of dynamics). e, Representative smFRET trace of real time TRF2 binding at telomeric duplex (flow at ~10 sec) to the POT 1 pre-bound overhang. f, The heatmap (n>100) of POT1 bound state in absence (top) and presence (bottom) of TRF2 (flow at ~10 sec).

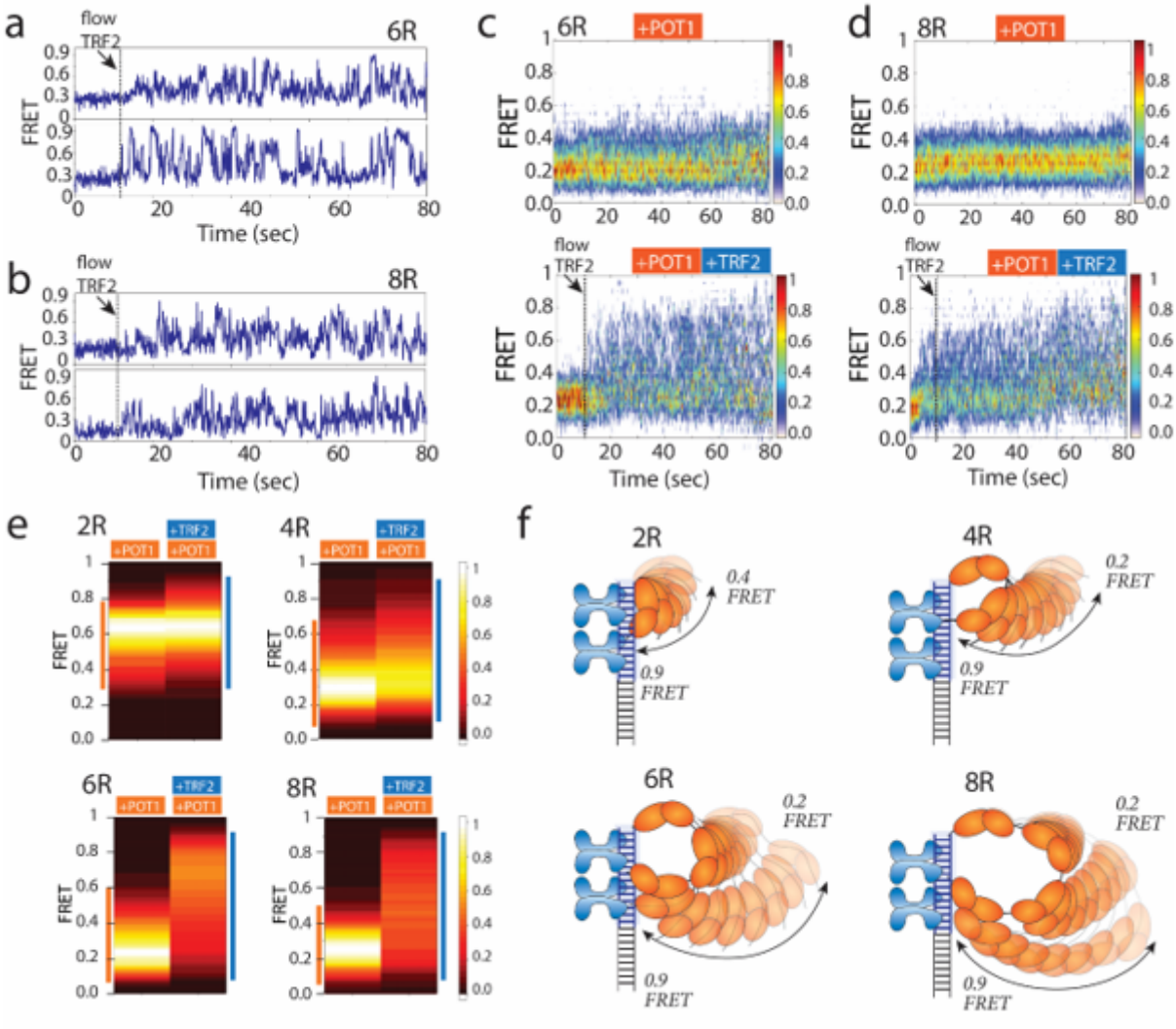

Figure 5

Enhanced dynamics also observed in longer telomeric overhang. (a & b), The representative real time smFRET traces of TRF2 binding at telomeric duplex (flow at ~10 sec) to the prebound POT1 of 6R (a) and 8R (b) overhangs. (c & d), The heatmap (n>100) of POT1 bound state in absence (top) and presence (bottom) of TRF2 (flow at ~10 sec) of 6R (c) and 8R (d) overhangs. e, FRET heatmap histograms generated from the dynamic traces of POT1 only and POT1 followed by TRF2 addition to 2R, 4R, 6R, and 8R overhangs containing telomeric duplex. f, Proposed model of TRF2 induced POT1 overhang dynamics of the respective construct.

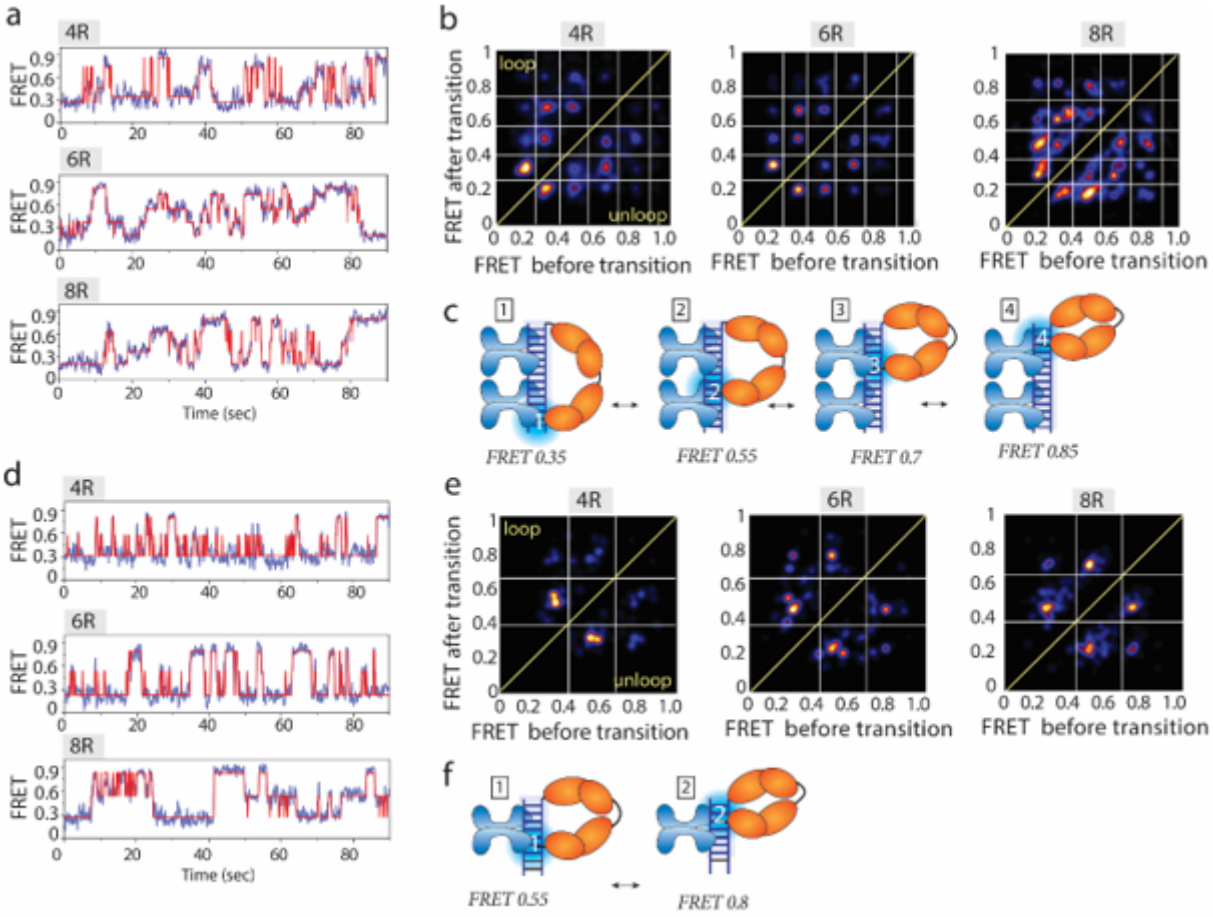

Figure 6

POT1 bound overhangs show discrete steps of moving up and down along the TRF2 bound duplex. (a & d), Representative smFRET traces (blue) fitted by HMM (red), (b & e), transition density plot (TDP) and, (c & f), the proposed models of POT1 bound 4R, 6R, and 8R telomeric overhangs moving up and down to the TRF2 bound four (a-c) and two (d-f) repeats of TTAGGG containing duplex.

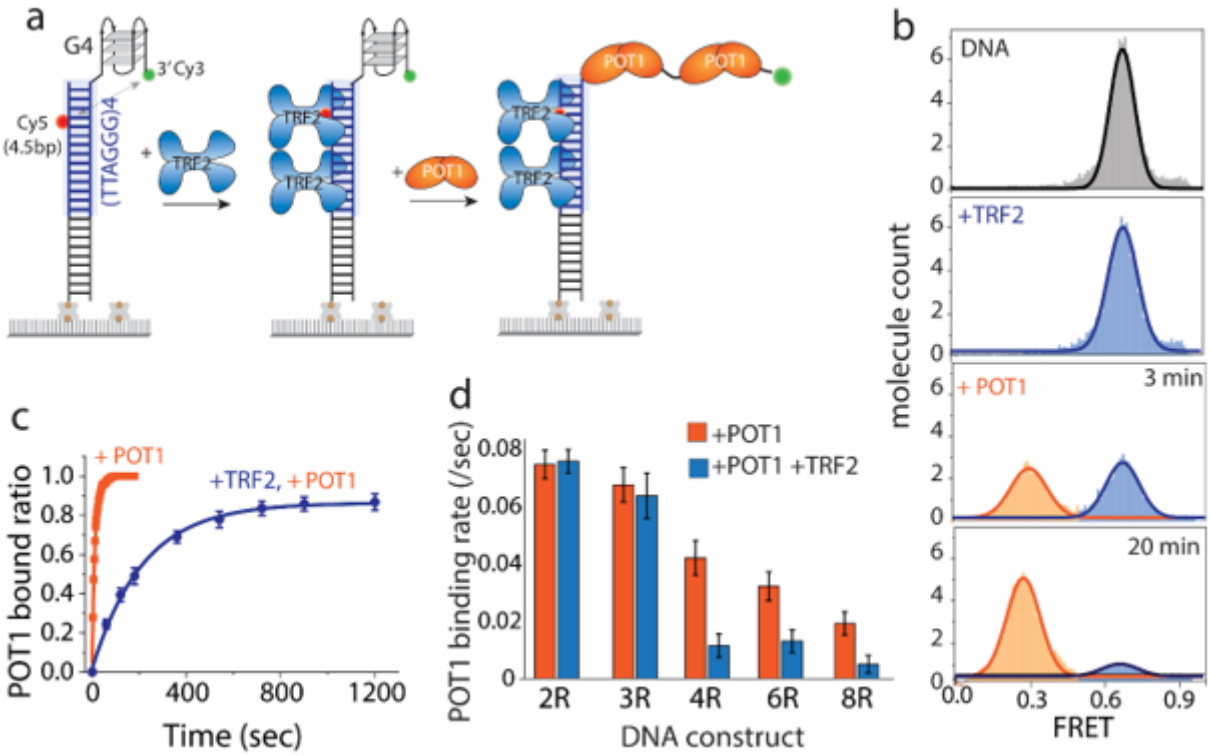

Figure 7

Telomeric duplex bound TRF2 delays POT1 binding to telomeric overhangs. a, Schematic model of telomeric duplex (four repeats of TTAGGG tract) with the G4/4R overhang, sequentially binding TRF2 at the duplex followed by POT1 at the overhang. b, The FRET histograms of telomeric duplex with 4R (top), TRF2 bound condition (second from top), and POT1 binding at 3 and 20 minutes respectively (bottom two). c, Single-exponential fitting of POT1 bound fraction in the absence and presence of TRF2. d, The bar graph represents the corresponding POT1 binding rate in the absence and presence of TRF2.

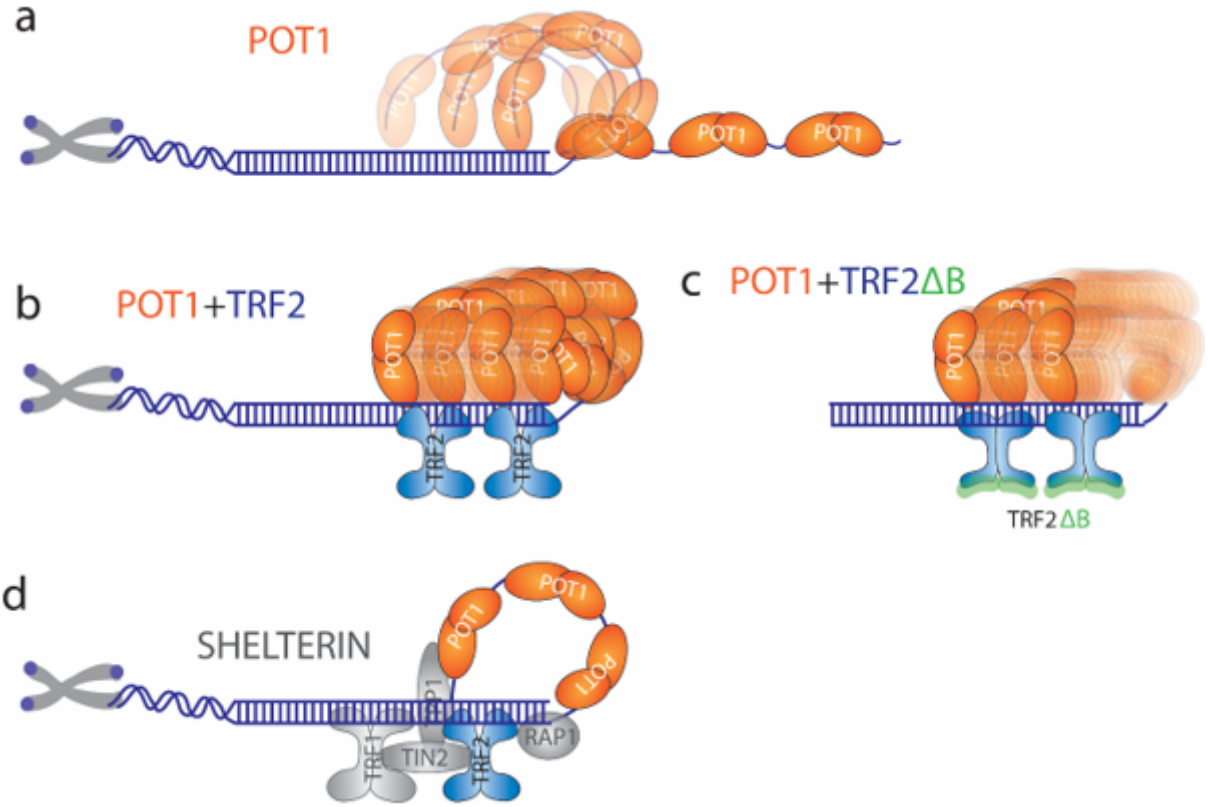

Figure 8

Proposed model of TRF2 and POT1 contributing to t-loop formation. a, POT1 bound telomeric overhang showing dynamics. b, TRF2 recruit POT1 bound 3’ end towards the junction and moving up and down along the duplex axis. c, TRF2ΔB doesn’t recruit POT1 bound 3’ end towards the junction. d, Shelterin components are expected to complete the stable t-loop formation.

Supplementary Files

This is a list of supplementary files associated with this preprint. Click to download.

- SUPPLEMENTARYINFORMATION.docx